USMS
019511 A Stochastic Study of Horizontal Two-Phase Flow

T. Darwich, Imperial C. of Sci. Tech & Med; H. Toral, Imperial C. of Sci. & Tech.; J.S. Archer, Imperial C. of Sci. Tech & Med

A Stochastic Study of Horizontal Two-Phase Flow

T. Darwich, H. Toral and J. S. Archer
Department of Mineral Resources Engineering
Imperial College of Science, Technology and Medicine

Abstract

The study presents stochastic features of pressure and void fraction turbulent waveforms in two-phase horizontal air-water flow. Amplitude and frequency domain features of the waveforms were shown to exhibit characteristic contour map surfaces on superficial air-water velocity coordinates.

Introduction

There are many multiphase flow regime studies in the literature which propose flow regime maps on the basis of empirical-visual observations (e.g. Baker[1], Mandhane *et al.*[2], Weisman *et al.*[3] and Spedding and Nguyen[4]) and/or mechanistic force balances (Taitel and Dukler[5] and Chisholm[6]).

There are also a number of studies where pressure and void fraction waveforms have been analysed by stochastic methods to discriminate between the different flow regimes (e.g. Hubbard and Dukler[7], Nishikawa *et al.*[8], Jones and Zuber[9], Vince and Lahey[10], Matsui[11, 12,13], Annuziato and Girardi[14,15,16] and Sekoguchi *et al.*[17]).

In our study we have taken the stochastic treatment of the turbulent pressure and void fraction waveforms one step higher by applying signal analysis methods employed in other disciplines such as voice recognition, seismic and medical diagnostics. These methods have enabled us to derive new "stochastic features" characterising the flow. We quantified the relative strength of these

features with reference to a common numeric scale. The features were plotted as contour maps on the superficial air-water velocity domain. The gradual grading of the feature contours gave a true representation of the flow regime changes. It is proposed that the feature maps could in time replace the customary visual flow maps. Visual flow maps fail in two respects: first, the flow regimes contain many more tones of grey than the eye can distinguish and usual vocabulary can describe and secondly, visual observations are heavily influenced by subjective bias.

Predictably, our study of "stochastic features" in two different diameter pipes has also failed in one respect. Each pipe exhibited a unique distribution of features (contour maps). Further research is in progress to discover features which are independent of flow configuration (i.e. upstream, downstream disturbances, pipe diameter and inclination, fluid physical properties *etc.*). The study nevertheless provides a necessary stimulus for an advance in flow characterisation and prediction.

Description of Experiments

a. Test Rig

A schematic diagram of the horizontal two-phase flow loop is shown in Fig. 1. Water flowrate was measured with an orifice and compressed air flowrate with a rotameter or an orifice.

Two separate 8.8 m long test sections of 50.0 mm I.D. and 26.0 mm I.D. pipe were employed. The stabilisation length between the point of mixing and the measurement section was equivalent to 113 diameters for the 50.0 mm I.D. pipeline and 217 diameters for the 26.0 mm I.D. pipe. Table 1 shows the range of flowrates employed in the tests

Table 1 Range of flow rates employed in the tests

ID	Superficial Water Velocity	Superficial Air Velocity
mm	m/s	m/s
50	0.072 - 3.405	0.266 - 8.509
26	0.282 - 3.360	0.115 - 8.621

Within this range all flow regimes can be obtained with the exception of annular flow. All measurements were carried out at near atmospheric conditions.

b. Measurements

The following sensors were installed on the 50 mm I.D. pipe: two absolute pressure transducers, three differential pressure transducers, void fraction capacitance transducer and a conductance probe. Fig. 1 shows the arrangement of the sensors.

The absolute pressure transducers were located at 117.5 D (587.5 cm) and 122 D (610 cm) from the mixing section. The differential pressure transducers were installed with three different tapping configurations; vertical cross section located at 113.2 D (566 cm), 1 D (5.0 cm) axial separation with the upstream tap at 131 D (655 cm) and 8.4 D (42 cm) axial separation with the upstream tap at 149.8 D (749 cm) from the mixing section.

The capacitance transducer consisted of two metal bands of width 8 mm and separation 10 mm connected to a capacitance meter. The voltage output from the meter was sampled as a faithful representation of the void fraction time record with respect to the "void fraction waveform features" , but no attempt was made or needed to measure the actual void fraction.

The conductance probe consisted of two miniature teflon coated stainless steel sensing elements of 0.075 mm diameter axially separated by 10mm. The holder tube acted as the reference sensor and the output voltage from the two sensor wires varied from a high value (air phase) to a low value (liquid phase). An optimum threshold voltage was determined to distinguish between the liquid and the vapour phases in a separate study of the performance of the miniature conductance probe. In this study void fraction measured by the micro probe was compared with the bulk average void fraction determined with quick closing valves.

The conductance probe was fitted to the test section with a special probe holder assembly which allowed the probe to be traversed along any radial direction.

c. Data Aquisition System

Measurements were digitised with an analog to digital converter controlled by a personal computer. Special menu driven software was developed for data sampling, plotting and filtering. The analog/digital converter employed a 12 bit digitiser with a maximum sampling frequency of 20 KHz through one channel and had a capability for simultaneous sampling through up to 8 channels at a lower sampling frequency.

The digital filtering software allowed the design and implementation of lowpass, highpass, bandpass and bandstop recursive or non-recursive filters to isolate the extraneous noise from the sampled waveforms.

Stochastic Features

Definitions and equations of the stochastic features used to characterise the turbulence waveforms are given in the appendix. The following gives a list of these features.

- Amplitude domain features: Probability density function, standard deviation, coefficient of skewness, coefficient of kurtosis.

- Frequency domain features: Linear prediction coefficients (Atal & Hanauer[18] and Makhoul[19])

Preliminary Studies of Signal Quality

a. Optimum Sampling Frequency

According to the sampling theorem, a waveform must be sampled at a frequency greater than or equal to double the highest frequency component of the waveform.

A study of the frequency spectrum of the pressure and void fraction signals across the full range of flow regimes attainable in this study showed that the informative range of the signal spectrum was contained below 20 Hz (Fig. 2). Thus, the optimal sampling frequency was selected as 40 Hz.

b. Optimal Record Length

In this study, the sample record was divided into a number of sections (blocks). Each one of the statistical features listed above was extracted from each block. The number of blocks was varied to check the effect of record length on the

average value of the features. The optimum record length was determined to be 256 points in a block and 16 blocks in the record.

c. Optimal Linear Predictor Order

The appropriate selection of the linear predictor order is usually based on the normalised error, V_p, which is defined as the ratio of the minimum error E_p to the energy in the signal R(0) (see appendix for the definition of E_p) :

$$V_p = \frac{E_p}{R(0)} \qquad (1)$$

A simple test to obtain the optimal linear predictor order is to check the V_p-p relationship (Fig. 3) which will almost be flat for $p > p_o$, where p_o is the optimal linear predictor order. Based on the linear prediction analysis of different signals, the optimum predictor order was selected to be 4.

d. Feature Quality - A qualitative study

Absolute pressure, differential pressure, void fraction (from capacitance transducer and conductance microprobe) waveforms in stratified, stratified wavy, plug, slug and bubbly flow regimes were analysed in the amplitude, frequency and time domains in a preliminary study to assess signal quality and the effectiveness of the statistical features.

The absolute pressure probability density function distributions (with zero mean) of the different flow regimes are shown in Fig. 4. The distributions are approximately normal for the different flow regimes with a slight distortion in the cases of plug and slug flows. The standard deviation, coefficient of skewness

and coefficient of kurtosis are used as quantitative measures of the probability density function.

Fig. 5a shows the the variation of the absolute pressure amplitude domain feature with sample block and flow regime. It is clear from this figure that there is a specific range of standard deviation value associated with each flow regime. The slug flow is characterised by high standard deviation while stratified and stratified wavy regimes are represented by low standard deviation. There was some degree of overlapping of the ranges of the coefficient of skewness and coefficient of kurtosis for the different flow regimes. This overlapping may be attributed to the relatively narrow range over which these coefficients are changing.

Frequency domain analysis of the absolute pressure signal with the linear prediction technique yields five features as the linear predictor coefficients a_1, a_2, a_3, a_4 and the normalised minimum total squared error, V_p.

Fig. 5b illustrates that the V_p feature can be used successfully to distinguish the separated flow regimes (stratified and stratified wavy) from the rest of the flow regimes. The stratified and stratified wavy flow regimes are usually associated with high values of Vp. On the other hand, plug, slug and bubbly flow regimes are generally associated with low values of V_p. Fig. 5c shows that the predictor coefficient a_1 can discriminate bubbly flow regime from the other flow regimes. It also shows that separated flow regimes (stratified and stratified wavy) tend to have a high value of a_1 while intermittent flow regimes (slug and plug) have a low value of a_1. The linear predictor coefficients a_2, a_3 and a_4 (Fig. 5d for a_2) exhibit a similar behaviour to V_p and a_1 in defining a particular level for separated flow regimes and a different one for intermittent flow regimes.

Time domain analysis of the absolute pressure signals with the autocorrelation function or cross correlation function between the absolute time records did not yield any significant information to differentiate between the flow regimes.

e. Feature Quality - A quantitative study

In order to evaluate the selected statistical features in terms of their ability to discriminate the different flow conditions over the ranges of superficial gas and liquid velocities investigated in this study, the F ratio used by Atal[20], in automatic speaker recognition was implemented. For a single statistical feature, the F ratio has been defined as :

$$F = \frac{\text{variance of speaker means}}{\text{average within speaker variance}}$$

$$= <[\,\bar{x}_i - \bar{\mu}\,]^2>_i \;/\; <[\,x_\alpha^{(i)} - \bar{x}_i\,]^2>_{\alpha,\,i} \qquad (2)$$

In our case of two-phase gas-liquid flow in pipelines, the "speaker" in the F ratio equation will be substituted by "flow condition". In equation 2, $x_\alpha^{(i)}$ is the feature value from the αth block of the signal representing the ith flow condition, which may be regarded as samples from a probability distribution associated with that specific flow condition. The symbol $< >_i$ indicates averaging over various flow conditions, $< >_\alpha$ indicates averaging over the different blocks of a single flow condition and $\bar{x}_i$ is the estimated mean value of the feature for the ith flow condition, i.e.

$$\bar{x}_i = < x_\alpha^{(i)} >_\alpha \qquad (3)$$

Finally, $\overline{\mu}$ is the overall mean value of the feature averaged over all flow conditions, i.e.

$$\overline{\mu} = < \overline{x}_i >_i \qquad (4)$$

It is obvious that for accurate recognition, a good feature is one for which the distributions of the different flow conditions are concentrated at widely different locations in the feature space. Consequently, the more suitable the feature, the higher the value of *F*.

The *F*-ratio values for the different absolute and differential pressure signals of the 50 mm pipeline are given in Table 2.

Table 2 *F*-ratio of absolute and differential pressure signal features

Feature	*F*-ratio			
	Absolute pressure	Radial differential	Axial - differential	
			1 D	8.4 D
SD	29.0	53.2	39.6	60.5
CS	2.00	0.28	0.12	1.66
CK	0.63	0.76	0.53	1.18
V_p	2.90	5.09	3.42	2.79
a_1	5.30	5.48	6.29	2.01
a_2	4.00	2.23	6.61	1.15
a_3	2.00	0.95	2.21	0.57
a_4	1.90	2.10	4.07	0.94

Feature Contour maps

Waveforms were sampled and analysed on a total of 545 points in the 50 mm pipe and 370 points in the 26 mm pipe and feature contour maps were obtained on superficial water-air velocity coordinates by an objective algorithm (Davis[21]).

1. Feature Contour maps for 50 mm pipe

Absolute Pressure Signal

Figs. 6 a-d represent some of feature contour maps for the absolute pressure signals (A complete list of the feature contour maps is presented by Darwich[20]). Fig. 6a shows that the standard deviation (SD) is mainly dependent on the superficial gas velocity with a sharp increase in the value of standard deviation at superficial gas velocities greater than 1.0 m/s and superficial liquid velocities between approximately 0.4 and 2.0 m/s. The sharp increase in the value of the standard deviaton in this range of gas and liquid velocities may be attributed to the formation of liquid slugs which are accompanied by a large variation in pressure before and after the slug. Fig. 6b shows the response of the coefficient of skewness to the variation of gas and liquid superficial velocities. It is clear that the coefficient of skewness is more sensitive to superficial liquid velocities than superficial gas velocities especially at high superficial gas velocities. The coefficient of kurtosis is less informative, showing a slight dependence on liquid velocities at low liquid flow rate.

The distribution of the linear prediction parameters V_p, a_1, a_2, a_3 and a_4 demonstrates an obvious dependence on the superficial gas and liquid velocities. While, V_p and a_1 are sensitve to the liquid velocity at high superficial liquid velocities (Figs. 6c-d), a_2, a_3 and a_4 are affected by the superficial gas velocity

at superficial liquid velocities less than 1.0 m/s and superficial gas velocities greater than 1.0 m/s.

Table 2 shows that the standard deviation is an outstanding feature of the absolute pressure waveform. The linear prediction parameters a_1 and a_2 can also be of use in certain ranges of the flow domain.

Radial Differential Pressure Signal

The distributions of some of the various statistical features associated with radial differential pressure signals are shown in Figs. 7a-d. The standard deviation (Fig. 7a) demonstrates an obvious dependence on the superficial gas and liquid velocities as for the absolute pressure.

The distributions of the linear prediction parameters V_p, a_1 and a_2 (Figs. 7b-d) also indicate a significant response to velocity variations throughout the tested flow domain. The distributions of other statistical features do not exhibit a definitive response to changes in flow velocities under most flow conditions.

Table 2 indicates that the standard deviation and the linear prediction parameters V_p and a_1 are seen to be the most effective features of the radial pressure waveform.

Axial Differential Pressure Signals

Table 2 presents the *F*-ratios of the axial differential pressure statistical features. Full contour maps for these features can be found in Darwich[22].

Table 2 shows that for differential pressure tapping waveforms obtained by 1D axial separation, the standard deviation and the linear prediction coefficients a_1 and a_2 are the most effective features

The *F*-ratio for the wider differential pressure tapping waveforms confirms the primary position of the standard deviation in the feature league table. The improvement of the *F*-ratio from 1D to 8.4D tapping separation is noteworthy. The effect of a wider tapping separation is also beneficial to the other amplitude domain features (CS and CK). The deterioration of the strength of the linear prediction parameters can be attributed to the dissipation of the turbulence structures in the longer run between the two measuring points.

Capacitance Transducer Void Fraction Signal

The distribution maps of the amplitude domain features are given in Figs. 8a-c. In general, these show a good response to variations in gas and liquid velocities. The standard deviation stands out as the strongest feature again.

b. Feature contour maps for 26 mm pipe

Absolute Pressure Signal

Absolute pressure feature maps for 26 mm I.D. pipe (Figs. 9 a-d) were plotted using the same isoline values used for the 50 mm I.D. pipe. In general, most of the statistical features appear to be more sensitive to the superficial gas velocity than to the liquid superficial velocity in the tested range which is mainly the intermittent flow region. The standard deviation distribution shows a distinctive dependence on the superficial gas velocity, a phenomenon that has been established with all pressure signals in the 50 mm I.D. pipe. The linear prediction coefficients, a_1, a_2 and a_3 also show significant dependence on superficial gas velocities, specifically with increasing gas velocities. The distribution map for the linear prediction coefficient V_p proves the effectiveness of V_p as a superficial liquid velocity dependent feature (Fig. 9c). Finally, the

amplitude domain features CS and CK as well as the linear prediction coefficient a_4 seem to be less informative as they show little response to the variations in the gas and liquid superficial velocities.

Radial Differential Pressure Signal

Radial differential pressure feature maps (Figs. 10a-d) were plotted using the same isoline values used for the 50 mm I.D. pipe.

In the main, the feature maps for the 26 mm I.D. pipe (Figs. 9 and 10) and the 50 mm I.D. pipes (Figs. 7 and 8) indicate similar trends but they do not coincide because the flow structures produced at the same superficial velocities are not identical for the two pipes and consequently different fluctuation characteristics are detected in the pressure signals.

Conclusions

1) Significant information can be obtained about the nature of two phase flow by statistical analysis of absolute pressure, differential pressure and void fraction turbulent waveforms.

2) A new set of stochastic features were extracted from the absolute and differential pressure signals using the Linear Prediction Technique to characterise flow conditions.

3) The time domain features (autocorrelation and crosscorrelation coefficients) of the pressure signals are less informative in characterising the flow conditions.

4) Measurements conducted over a wide range of superficial gas and liquid velocities have resulted in a set of stochastic feature contour maps which illustrate varying degrees of sensitivity to gas and liquid superficial velocities.

5) The *F*-ratio was used as a quantitative scale to measure the effectiveness of the stochastic features to characterise flow conditions.

6) It is suggested that the present technique can be extended to multi-phase systems containing oil-water-gas phases.

7) Feature maps showed same trends for different pipe diameters.

Nomenclature

a_1	linear prediction coefficient a_1
a_2	linear prediction coefficient a_2
a_3	linear prediction coefficient a_3
a_4	linear prediction coefficient a_4
CK	coefficient of kurtosis
CS	coefficient of skewness
E_p	minimum total squared error [Eq. 14]
e_t	residual error [Eq. 12]
G	system's gain
ID	inner pipe diameter (mm)
n	number of points
p(x)	probability density function
p_o	optimal linear prediction order
R(0)	energy in the signal
SD	standard deviation (cm of water)
u_t	unknow input of a hypothesized system in equation 9.

V_p	normalised linear prediction error [Eq. 1]
V_{sg}	superficial gas velocity(m/s)
V_{sl}	superficial liquid velocity(m/s)
x(t)	sample time history record
$\overline{x}$	mean
$\overline{\mu}$	overall mean value of the feature averaged over all flow conditions

References

1. Baker, O. : " Designing for simultaneous flow of oil and gas," *Oil & Gas J. (1954),* 53, no. 12, 185-195.

2. Mandhane, J. M., Gregory, G. A. and Aziz, K. : " A flow pattern map for gas-liquid flow in horizontal pipes," *Int. J. Multiphase Flow* (1974), 1, 537-553.

3. Weisman, J., Duncan, D., Gibson, J. and Crawford, T. : " Effects of fluid properties and pipe diameter on two-phase flow patterns in horizontal lines," *Int. J. Multiphase Flow* (1979), 5, 437-462.

4. Spedding, P. L. and Nguyen, V. T. : " Regime maps for air-water two-phase flow," *Chem. Eng. Sci.* (1980), 35, 779-793.

5. Taitel, Y. and Dukler, A. E. : " A model for predicting flow regime transitions in horizontal and near horizontal gas-liquid flow," *AIChE J.* (1976), 22, no. 1, 47-55.

6. Chisholm, D. : " Prediction of flow pattern boundaries in horizontal two-phase flow," *IChemE Sym. Series* (1986), 86, 761-772.

7. Hubbard, M. G. and Dukler, A. E. : " The characterization of flow regimes for horizontal two-phase flow," *Proceedings Heat Transfer and Fluid Mechanics Institute* (1966), 100-121.

8. Nishikawa, K., Sekoguchi, K. and Fukano, T. : " On the pulsation phenomena in gas-liquid two-phase flow (Relationship between pulsating pressure and flow pattern in upward two-phase flow), " *Bull. JSME* (1969), 12, 1410-1416.

9. Jones, O. C. and Zuber, N. : " The interrelation between void fraction fluctuations and flow patterns in two-phase flow," *Int. J. Multiphase Flow* (1975), 2, 273-306.

10. Vince, M. A. and Lahey, R. T. : " On the development of an objective flow regime indicator, " *Int. J. Multiphase Flow* (1982), 8, 93-124.

11. Matsui, G. : " Identification of flow regimes in vertical gas-liquid two-phase flow using differential pressure fluctuations," *Int. J. Multiphase flow* (1984), 10, 711-720.

12. Matsui, G. : " Identification of flow patterns in horizontal gas-liquid two-phase flow using differential pressure fluctuations," *Int. Symp. on Fluid Control & Measurement* (1985), Tokyo, Japan.

13. Matsui, G. : " Automatic identification of flow regimes in vertical two-phase flow using differential pressure fluctuations," *Nuclear Engineering and Design* (1986), 95, 221-231.

14. Annunziato, M. and Girardi, G. : " Flow pattern identification by pressure drop and void fraction fluctuations analysis in vertical two-phase flow," *Paper F4 at Eur. Two-phase Flow Group Mtg.* (19-21 June 1983), Rome, Italy.

15. Annunziato, M. and Girardi, G. : " Statistical methods to identify two-phase regimes: Experimental results for vertical large diameter tubes," *Paper G5 presented at 2nd. International Conference on Multiphase flow* (19-21 June 1985), London, England.

16. Annunziato, M. and Girardi, G. : " Horizontal two-phase flow : A statistical method for flow pattern recognition," *Paper presented at 3rd. International Conference on Multiphase Flow* (18-20 May 1986), The Hague, Netherlands.

17. Sekoguchi, K., Inoue, K. and Imasaka, T. : " Void signal analysis and gas-liquid two-phase flow regime determination by a statistical pattern recognition method," *Bull. JSME (1987),* 30, no. 266, 1266-1273.

18. Atal, B. S. and Hanauer, S. L. : " Speech analysis and synthesis by linear prediction of the acoustic wave," *J. Acoust. Soc. Amer.* (1971), 50, 637-655.

19. Makhoul, J. : " Linear prediction: A tutorial review," *Proc. IEEE* (1975), 63, no. 4, 561-580.

20. Atal, B. S. : " Automatic Recognition of speakers from their voices," *Proceedings IEEE* (1976), 64, no. 4, 458-475.

21. Davis, J. C. : " Statistics and data analysis in geology," John Wiley & Sons (1986).

22. Darwich, T. : " A Statistical Method for Two-Phase Flow Metering," *Ph. D. Thesis* (1989), Imperial College of Sci., Tech. and Medicine, U. of London.

23. Bendat, J. S. and Piersol, A. G. : *Random data : Analysis and measurement procedures.* Wiley-Interscience (1971).

24. Witten, I. H. : *Principles of computer speech.* Academic Press, London (1982).

APPENDIX - STOCHASTIC FEATURES

a. Amplitude Domain Features

The probability density function of a random signal describes the probability that the sampled data will assume a particular value within some defined range at any instant of time (Bendat and Piersol[23]). The probability density function, p (x), can be defined as follows :

$$p(x) = \lim_{\Delta x \to 0} \frac{\text{Prob}\left(x < x(t) < x + \Delta x \right)}{\Delta x}$$

$$= \lim_{\Delta x \to 0} \frac{1}{\Delta x} \left(\lim_{T \to \infty} \frac{T_x}{T} \right) \qquad (1)$$

where $p(x)$ is the probability density function of a sample time history record $x(t)$ and T is the observation time. The moments associated with the probability density function can be used as descreptive measures of the distribution. These moments are the mean (first moment about the origin), the standard deviation (second moment about the mean), the coefficient of skewness (third moment about the mean) and the coefficient of kurtosis

(fourth moment about the mean). The mean, x, is the average value of the data points and can be defined as follows :

$$\bar{x} = \frac{\sum_{i=1}^{n} x_i}{(n-1)} \qquad (2)$$

where n is the total number of points in the sampled record. The standard deviation is the root mean square of the deviations from the arithmetic mean and is a measure of the dispersion of the data. The standard deviation, SD, is defined as :

$$SD = \left(\frac{\sum_{i=1}^{n} (x_i - \bar{x})^2}{(n-1)} \right) \qquad (3)$$

When a distribution is not symmetrical about its mean value, it is said to be skew. If the tail of the distribution is longer on the right of the mode (the highest point on the distribution), the distribution is said to be skewed to the right or to have positive skewness. Similarly, if the tail is longer on the left, the distribution is skewed to the left or has negative skewness. The coefficient of skewness, CS, is defined as :

$$CS = \frac{\sum_{i=1}^{n} (x_i - \bar{x})^3}{(n-1)\ (SD)^3} \qquad (4)$$

Kurosis is the peakedness of a distribution. The normal curve is taken as the standard of peakedness. A curve less peaked than the normal is said to be platykurtic and a more peaked curve is said to be leptokurtic. The coefficient of kurtosis, CK, is defined as :

$$CK = \left(\frac{\sum_{i=1}^{n} (x_i - \bar{x})^4}{(n-1)\ (SD)^4} \right) - 3 \qquad (5)$$

b. Frequency Domain Features

A new frequency domain analysis technique for two-phase gas-liquid flow waveforms will be presented and utilised in this study. Atal and Hanauer[17] introduced the linear prediction method in speech processing which became increasingly dominant in speech analysis. Makhoul[18] presented a very informative review of the technique which will be briefly described in the following.

Linear prediction provides a simple and effective method to obtain the main characteristics of the spectral density function of the signal. In this technique, the signal is modeled as a linear combination of its past values and past and present values of a hypothetical input to a system whose output is the given signal. According to this model, the signal, x_t, can be represented in the following form :

$$x_t = -\sum_{k=1}^{p} a_k x_{t-k} + G \sum_{l=0}^{q} b_l u_{t-l}, \quad b_0 = 1 \qquad (6)$$

where a_k, $1 \le k \le p$, b_l, $1 \le l \le q$, and the gain G are the parameters of the hypothesized system with some unknown input u_t. Equation (6) can be rewritten in the frequency domain by taking the Z-transform of both sides that yields :

$$H(z) = \frac{X(z)}{U(z)} = G \frac{1 + \sum_{l=1}^{q} b_l z^{-l}}{1 + \sum_{k=1}^{p} a_k z^{-k}} \qquad (7)$$

where

$$X(z) = \sum_{t=-\infty}^{\infty} x_t z^{-t} \qquad (8)$$

is the Z-transform of x_t, U (z) is the Z-transform of u_t and H (z) is the transfer function of the system, which is the general pole-zero model. The roots of the numerator and denominator polynomials are the zeros and poles of the model respectively. There are two special cases of the model which are : 1) all-zero model where $a_k = 0$, $1 \leq k \leq p$; 2) all-pole model where $b_l = 0$, $1 \leq l \leq q$. The following section will be confined to the all-pole model which is going to be implemented in the current study.

In the all-pole model, equations (6) and (7) are reduced to:

$$x_t = -\sum_{k=1}^{p} a_k x_{t-k} + G u_t \qquad (9)$$

$$H(z) = \frac{G}{1 + \sum_{k=1}^{p} a_k z^{-k}} \qquad (10)$$

Since the output, u_t, is totally unknown, the output signal, x_t, can only be approximately predicted from previous samples, i.e.

$$\tilde{x}_t = -\sum_{k=1}^{p} a_k x_{t-k} \qquad (11)$$

Where $\tilde{x}_t$ is the approximation of x_t. The difference between the actual value x_t and the predicted value $\tilde{x}_t$ is called the residual error, e_t, which is given by :

$$e_t = x_t - \tilde{x}_t = x_t + \sum_{k=1}^{p} a_k x_{t-k} \qquad (12)$$

The predictor coefficients, a_k, should be adapted to minimise the error signal, e_t, which is achieved by the minimisation of the total squared prediction error with respect to the coefficients. The total squared error, E, is defined as :

$$E = \sum_t e_t^2 = \sum_t \left(x_t + \sum_{k=1}^{p} a_k x_{t-k} \right)^2 \qquad (13)$$

To minimize E with respect to each of the coefficients, equation (13) is differentiated with respect to a_i and set the resulting derivatives to zero. The minimum total squared error, E_p, can finally be given as :

$$E_p = \sum_t x_t^2 + \sum_{k=1}^{p} a_k \sum_t x_t \, x_{t-k} \qquad (14)$$

By solving the set of p equations, given in equation (14) in p unknowns, the linear prediction coefficients a_k which minimise the total squared error can be obtained. Makhoul[19] and Witten[24] give a thorough review of the methods used for the estimation of the linear prediction parameters. The linear prediction technique is to be implemented in the field of two-phase flow in a similar way to that applied in speech analysis. Since it provides a simple and effective method of representing different signals in terms of a small number of parameters, the linear prediction method can be used not

only as a way of data compression but also as a supply for different statistical features of the different two-phase flow conditions.

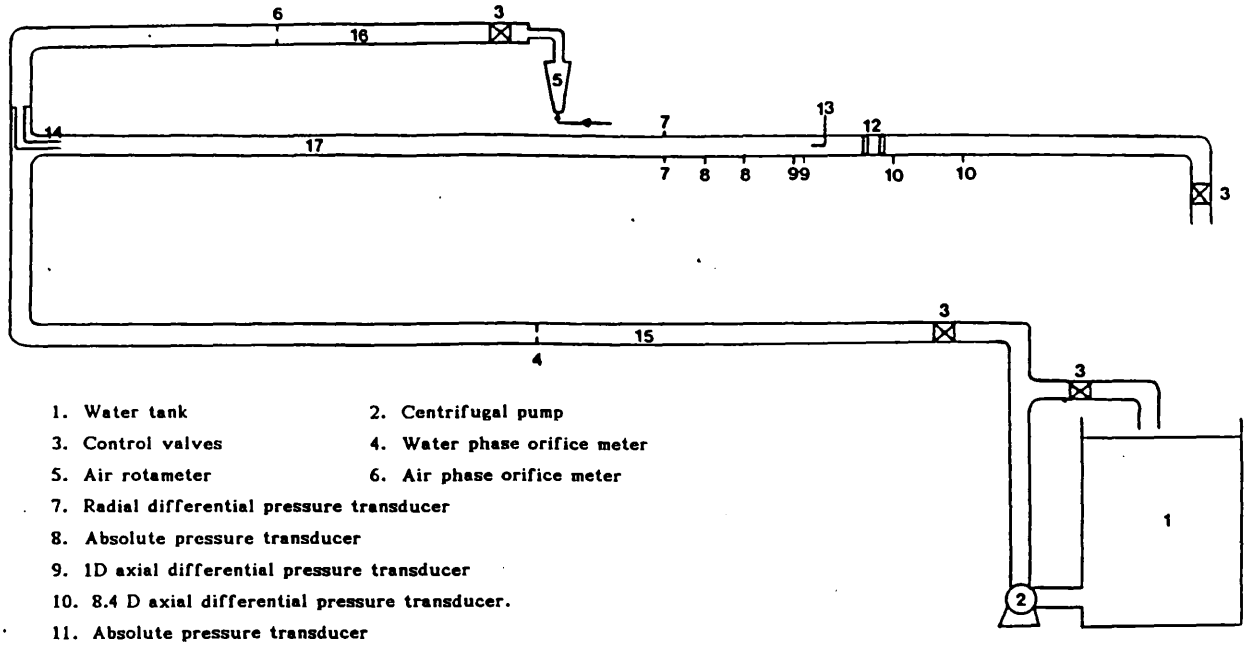

1. Water tank
2. Centrifugal pump
3. Control valves
4. Water phase orifice meter
5. Air rotameter
6. Air phase orifice meter
7. Radial differential pressure transducer
8. Absolute pressure transducer
9. 1D axial differential pressure transducer
10. 8.4 D axial differential pressure transducer.
11. Absolute pressure transducer
12. Capacitance transducer
13. Conductance probe
14. Mixing section
15. Single phase liquid flow line
16. Single phase gas flow line
17. Two-phase flow line

Fig. 1 Layout of experimental rig

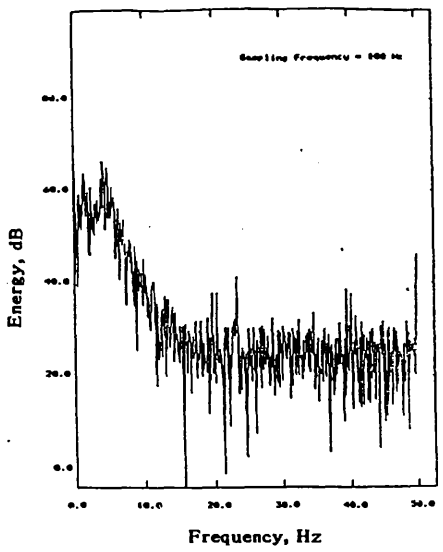

Fig. 2 Frequency spectrum of a radial differential pressure signal

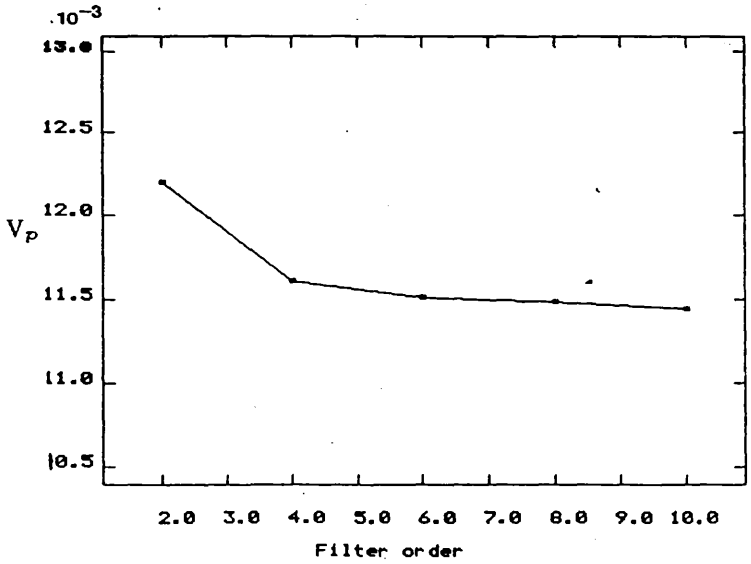

Fig. 3 Linear predictor order selection (slug flow)

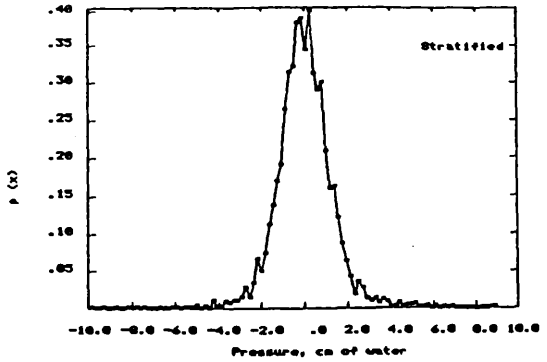

a) V_{sg}=0.359 m/s, V_{sl}=0.103 m/s

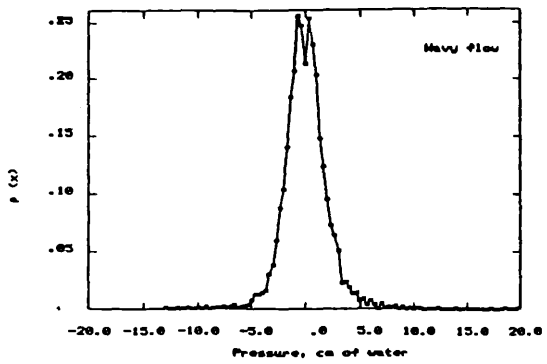

b) V_{sg}=6.142 m/s, V_{sl}=0.076 m/s

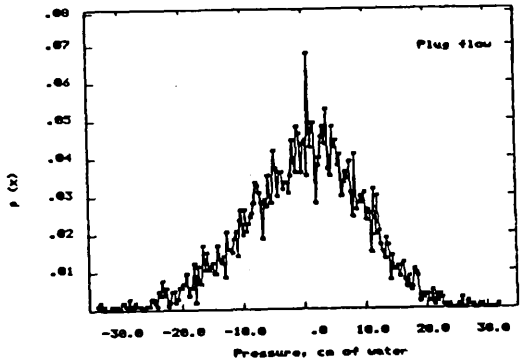

c) V_{sg}=0.644 m/s, V_{sl}=1.439 m/s

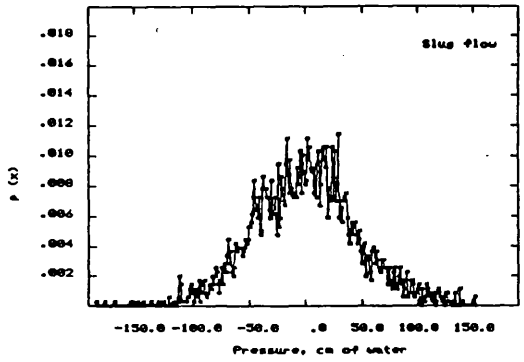

b) V_{sg}=3.666 m/s, V_{sl}=1.704 m/s

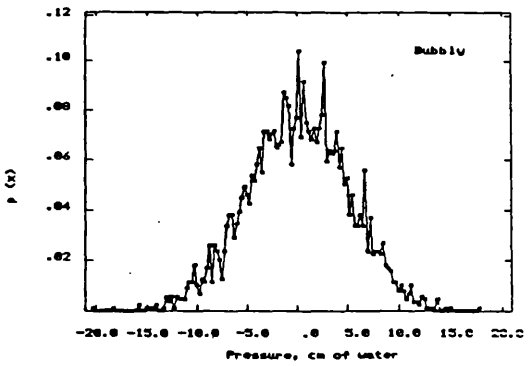

e) V_{sg}=0.677 m/s, V_{sl}=2.600 m/s

Fig. 4 The probability density function of the absolute pressure signal for different flow regimes.

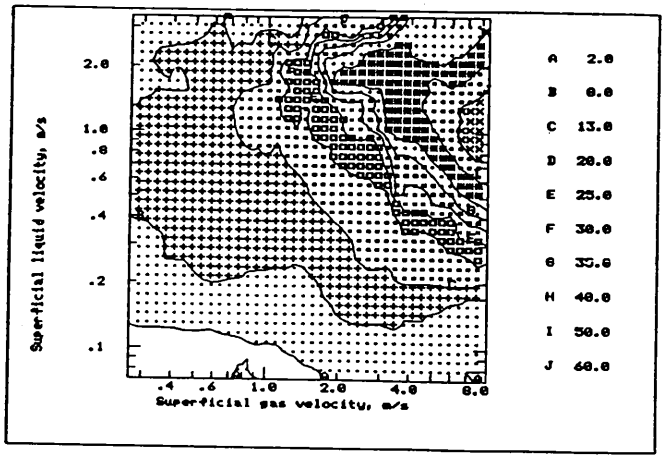

a) Standard deviation

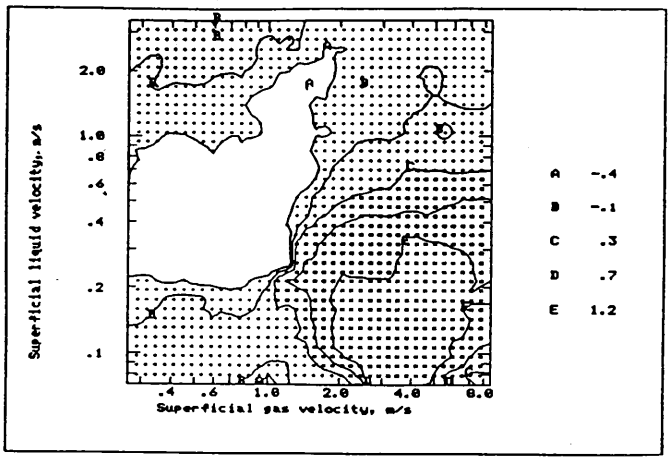

b) coefficient of skewness

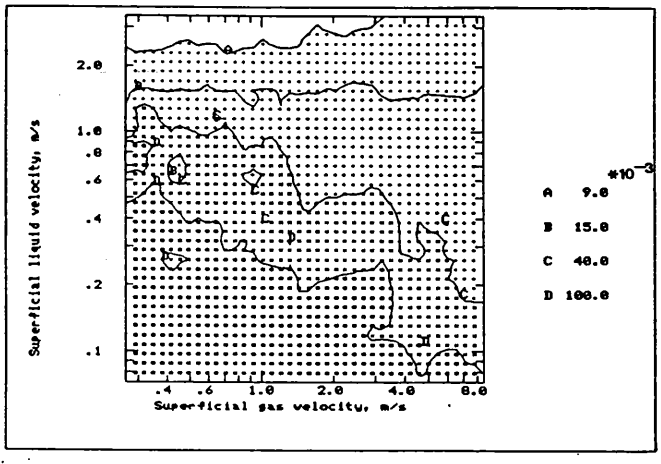

c) Linear prediction coefficient V_p

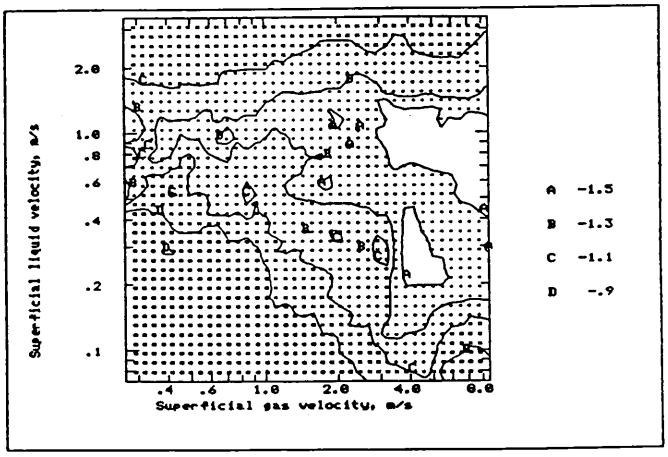

b) Linear prediction coefficient a_1

Fig. 6 Features contour maps for the absolute pressure signal

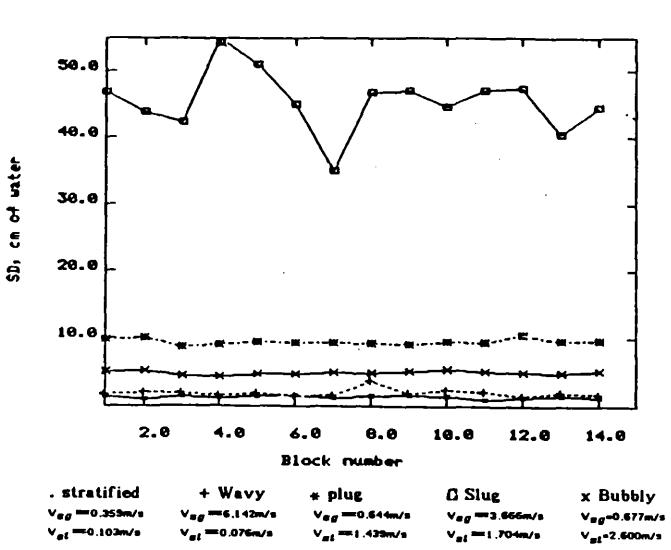

a) Standard deviation

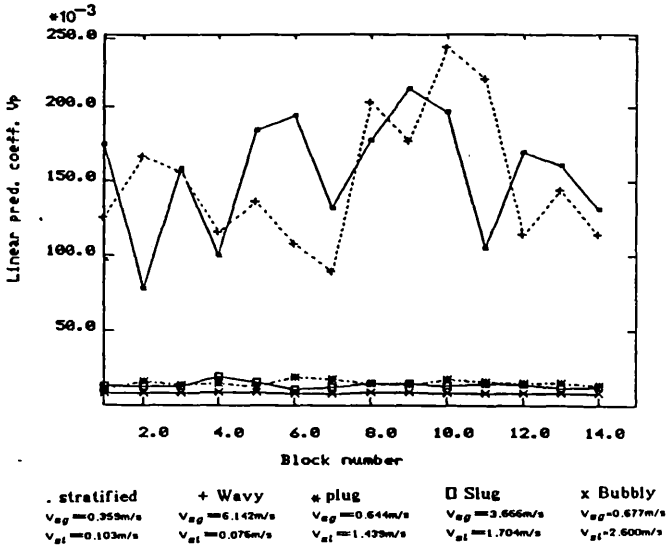

b) Linear prediction coefficient V_p

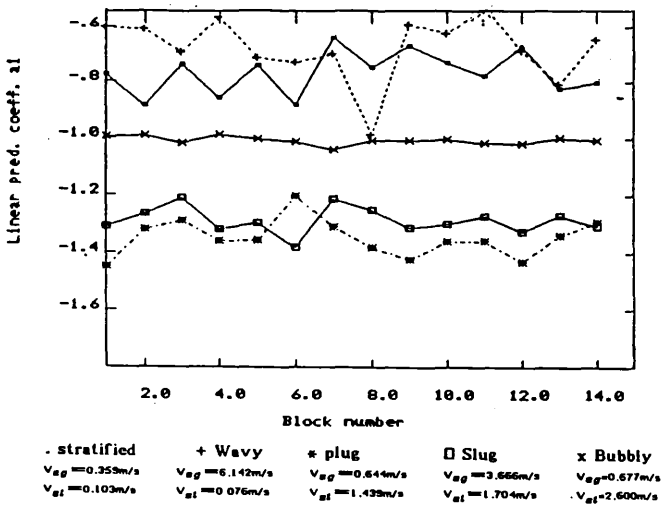

c) Linear prediction coefficient a_1

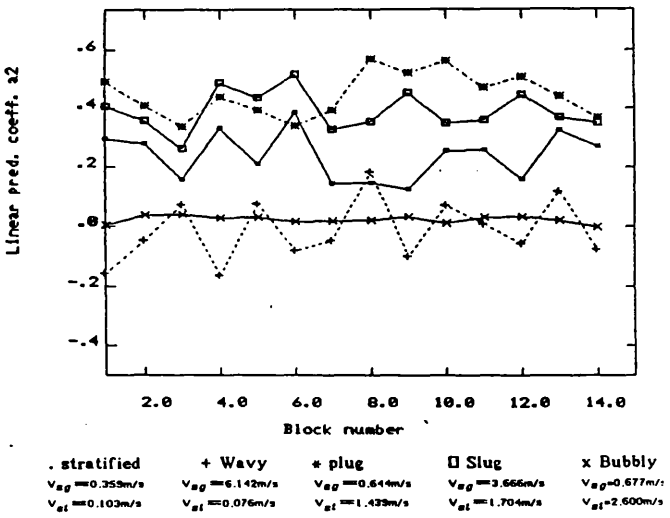

b) Linear prediction coefficient a_2

Fig. 5 Variation of the absolute pressure signal's features with sample block and flow regime.

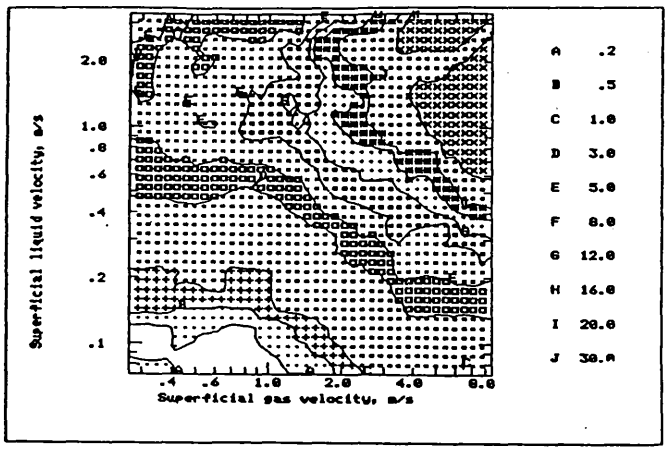

a) Standard deviation

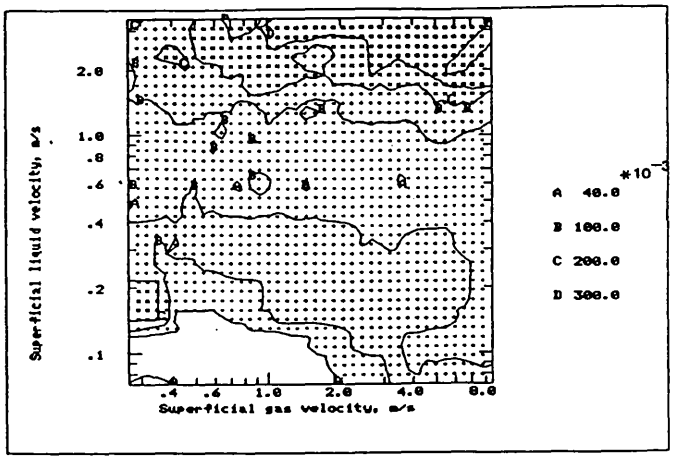

b) Linear prediction coefficient V_p

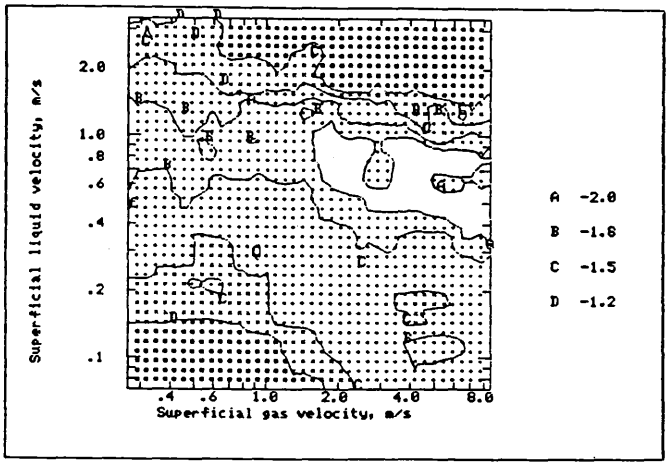

c) Linear prediction coefficient a_1

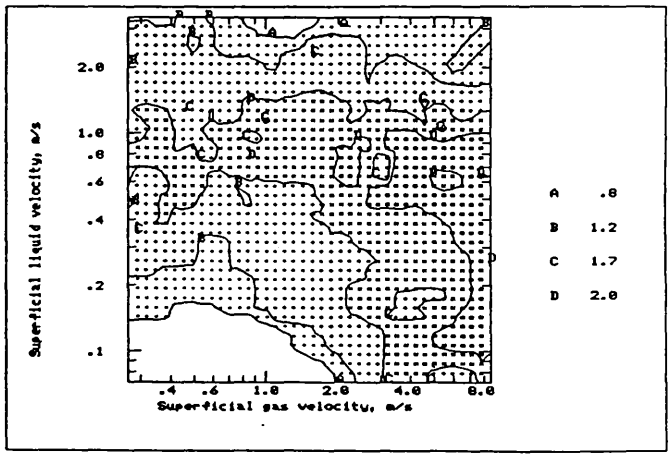

b) Linear prediction coefficient a_2

Fig. 7 Features contour maps for the radial differential pressure signal

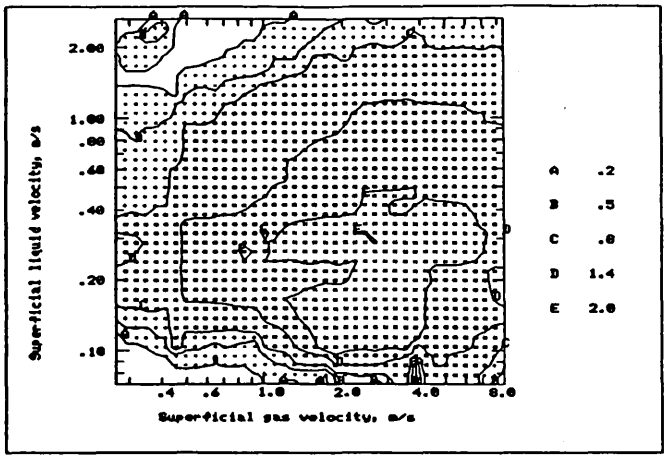

a) Standard deviation

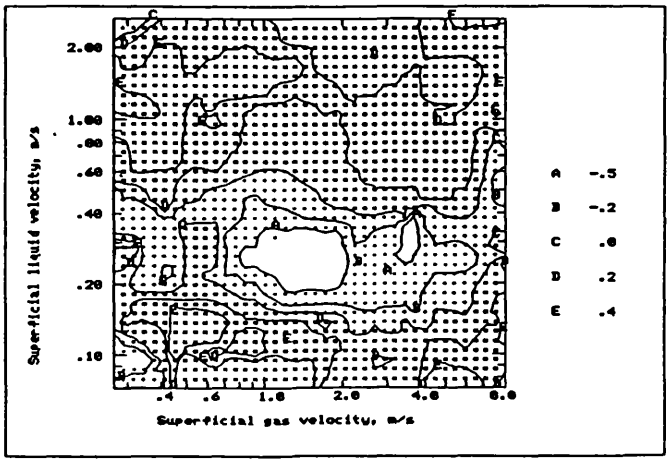

b) Coefficient of skewness

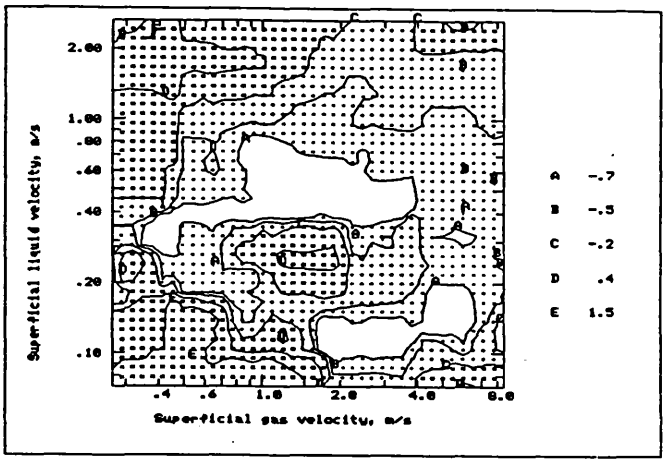

c) Coefficient of kurtosis

Fig. 8 Features contour maps for the capacitance transducer

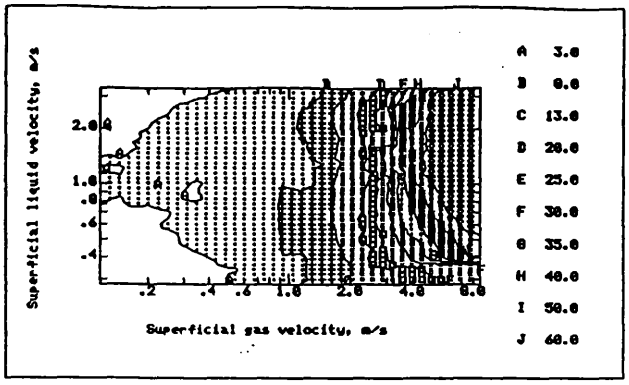

a) Standard deviation

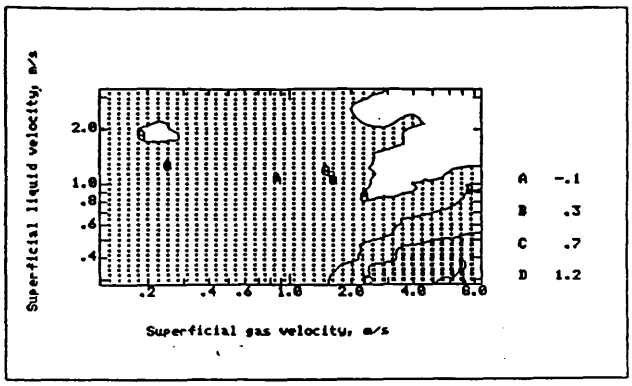

b) Coefficient of skewness

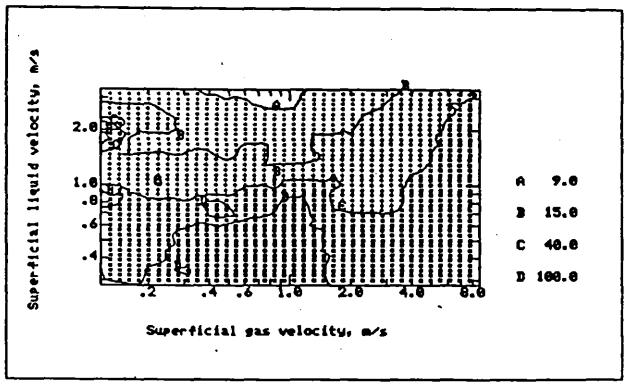

c) Linear prediction coefficient V_p

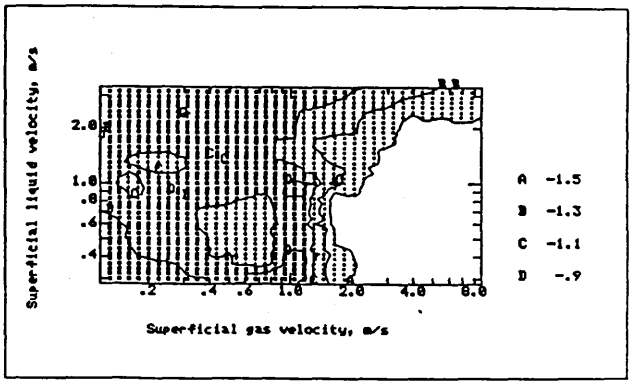

b) Linear prediction coefficient a_1

Fig. 9 Features contour maps for the absolute pressure signal (26 mm pipe)

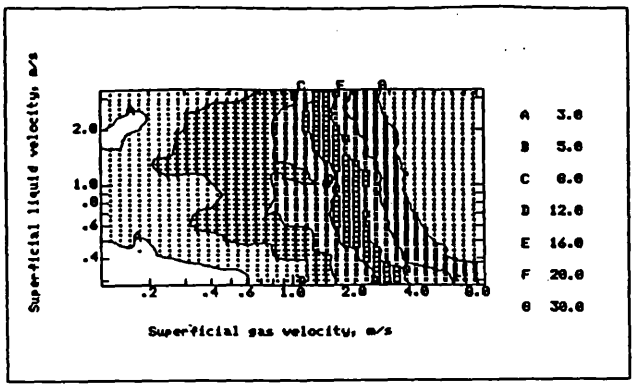

a) Standard deviation

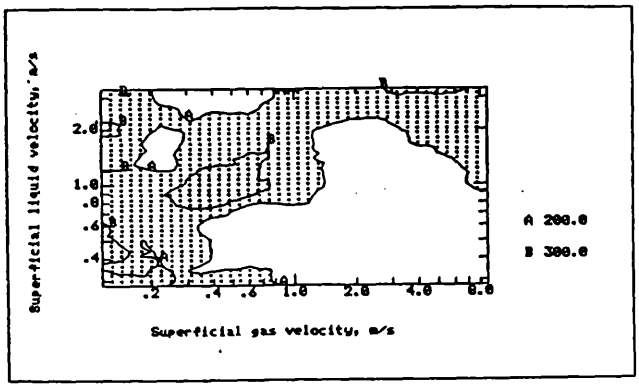

b) Linear prediction coefficient V_p

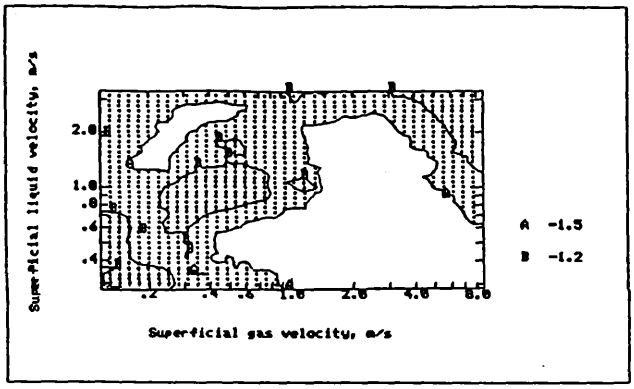

c) Linear prediction coefficient a_1

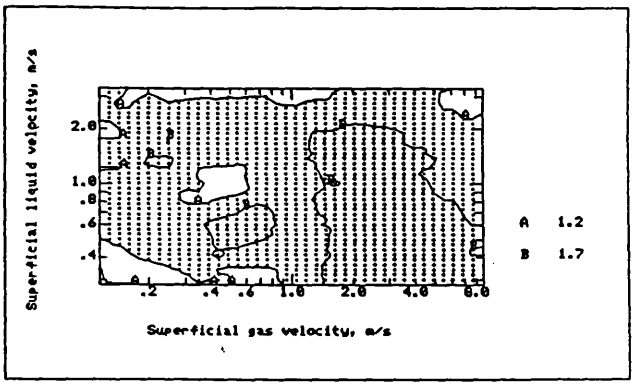

b) Linear prediction coefficient a_2

Fig. 10 Features contour maps for the radial differential pressure signal (26 mm pipe)